Electronic Supplementary Material (ESI) for Energy & Environmental Science
This journal is © The Royal Society of Chemistry 2013

Influence of Li_2O_2 Morphology on Oxygen Reduction and Evolution Kinetics in Li-O_2 Batteries

Betar M. Gallant, David G. Kwabi, Robert R. Mitchell, Jigang Zhou, Carl V. Thompson and Yang Shao-Horn

Supporting Information

Experimental Details

Electrode fabrication / catalyst preparation.

Catalyst Preparation: Si wafers (6" diameter, n-type doping, 140 nm thick thermal SiO_2) were prepared for catalyst deposition by cleaning using a Piranha solution (3:1 H_2O_2:HSO_4). Next, sequential layers of Al_2O_3 (30 nm) and Fe (1 nm) were deposited using electron beam evaporation without breaking vacuum between layer depositions. The catalyst wafers were then cleaved into small samples (~1 x 1 cm) in preparation for CNT growth.

Chemical Vapor Deposition: Multi-walled carbon nanotubes (CNTs) were synthesized in a two-furnace hot-walled thermal chemical vapor deposition system. The two furnaces are connected with a single quartz tube (OD 1"). The upstream furnace (preheater) is used to preheat the carbon precursor to promote gas decomposition and results in improved carbon nanotube growth. The downstream furnace (growth furnace) is where catalyst samples are located and CNTs are grown. The CNTs used in this study were synthesized using the process detailed in the main text. After the post-growth anneal the growth furnace was opened and the tube was rapidly cooled to room temperature under He flow. After cooling, the CNTs were removed from the furnace and then removed from the substrate by gently prying the corners of the monolithic carpet until the carpet uniformly delaminated from the growth substrate.

TEM sample preparation.

Small electrode fragments were prepared for TEM imaging by sandwiching them inside foldable TEM grids (Ted Pella, Stratatek) in order to minimize damage from sample preparation (i.e. samples were not sonicated). Sample preparation was performed inside an argon-filled glovebox and prepared grids were transported to the TEM in argon-filled airtight containers. Bright field zero-loss imaging was performed at an accelerating voltage of 120 kV in an energy-filtered Zeiss Libra 120 TEM.

XRD crystallite size analysis.

Average crystallite sizes of Li_2O_2 in discharged electrodes were determined by peak broadening analysis on raw XRD data (Fig. 3a and additional data) using the Scherrer equation assuming spherical crystallites[1]:

This journal is © The Royal Society of Chemistry 2013

$$t = \frac{0.9\lambda}{B\cos\theta_B}$$

where t is the crystallite broadening, λ is the radiation wavelength (1.54 Å for Cu Kα), θ_B is the Bragg angle, and B is the full width half maximum at $2\theta_B$. Due to the presence of a broad background shoulder from Kapton near the (101) peak at 34.97° 2θ, and to the presence of two closely spaced peaks at 58.72 and 58.98° 2θ, only the highest intensity (100) peak at 32.89° 2θ was used for crystallite size measurements. For commercial Li_2O_2 measurements, 90% phase-pure Li_2O_2 powder (with 10% LiOH, Sigma-Aldrich, USA) was ball-milled in a PULVERISETTE 6 (Fritsch, Germany) at 500 rpm without solvent under dry argon for 5 hours.[2]

This journal is © The Royal Society of Chemistry 2013

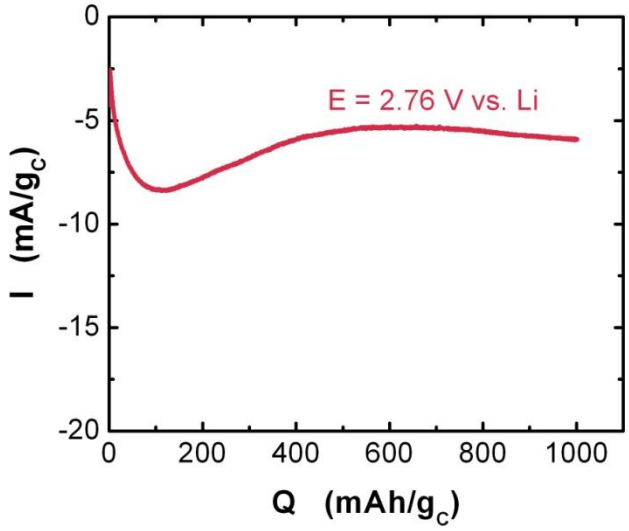

Figure S1. Representative potentiostatic discharge curve at 2.76 V vs. Li to 1000 mAh/g_C, forming a Li_2O_2 disc morphology.

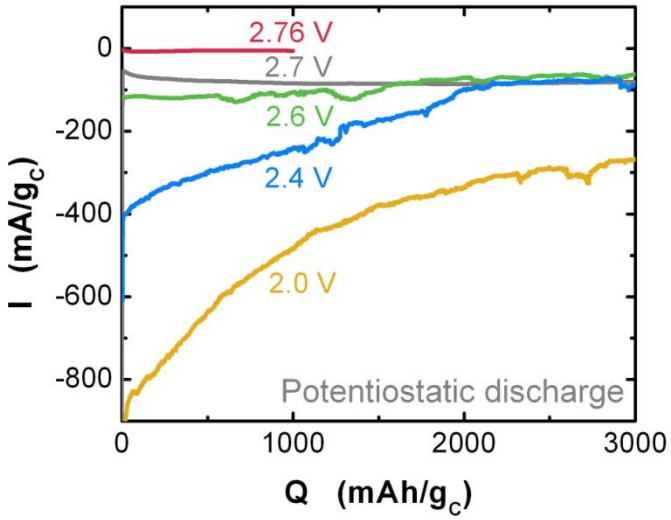

Figure S2. Current vs. capacity of CNT electrodes discharged potentiostatically over a range of potentials between 2.0 – 2.76 V vs. Li (same electrodes as shown in Fig. 1a but over a wider capacity range).

This journal is © The Royal Society of Chemistry 2013

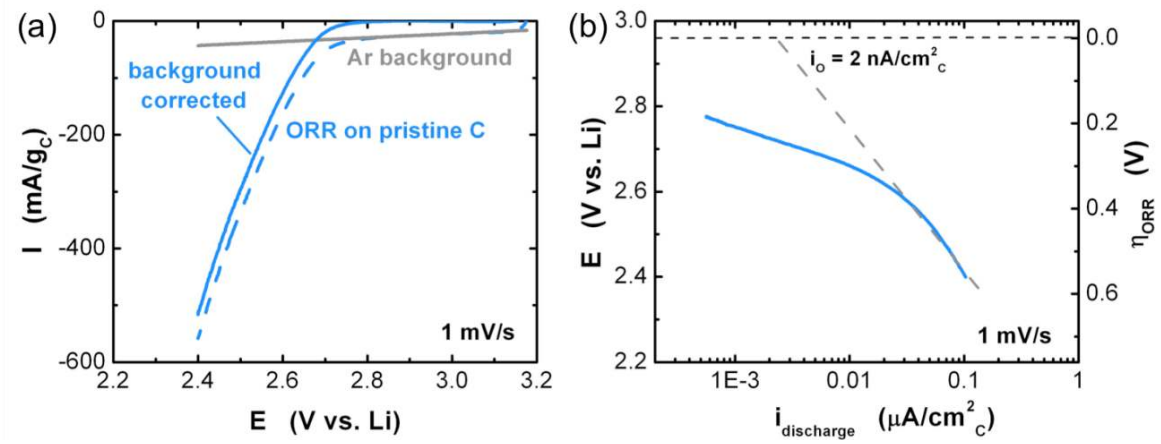

Figure S3. (a) Cyclic voltammetry scan of CNT electrodes starting at open circuit (3.2 V vs. Li) to 2.4 V vs. Li at a scan rate of 5 mV/s. The gray line shows the background in argon, while the blue lines show the raw data of the ORR current in oxygen (dashed blue line) and the capacitance-corrected ORR current obtained by subtracting the argon background (solid blue line). (b) Tafel plot of the capacitance-corrected ORR current (solid blue line in (a)) as a function of the discharge potential. The dashed line is a linear fit to the CV data below 2.6 V.

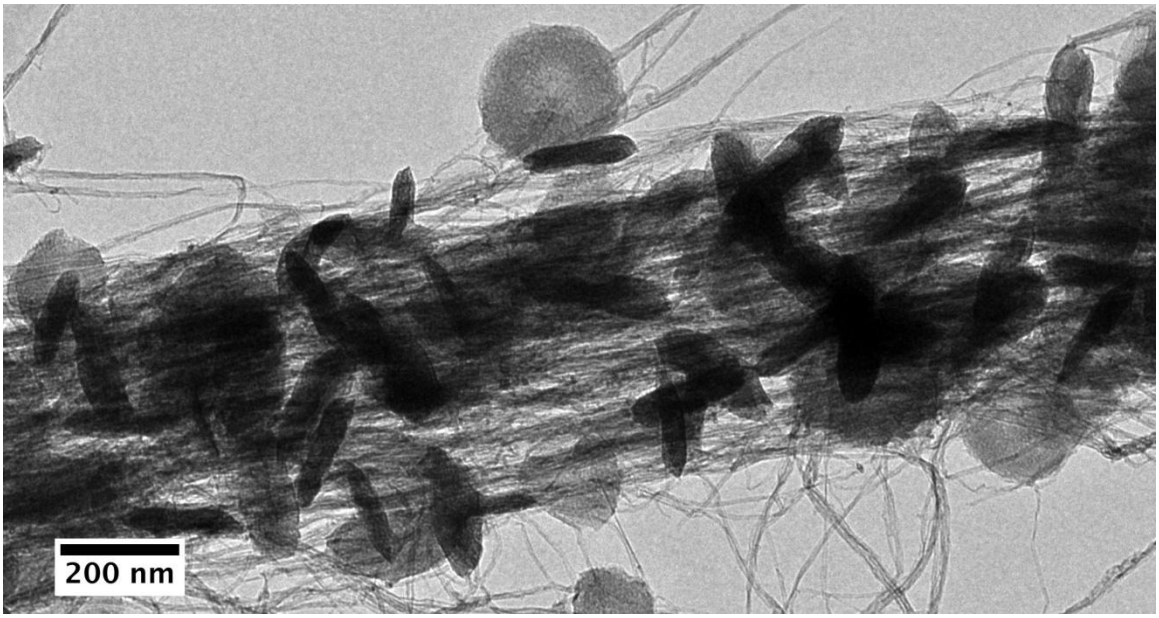

Figure S4. Low magnification TEM image of the electrode in Fig. 2a (E > 2.74 V to 2000 mAh/g_C, PITT discharge).

This journal is © The Royal Society of Chemistry 2013

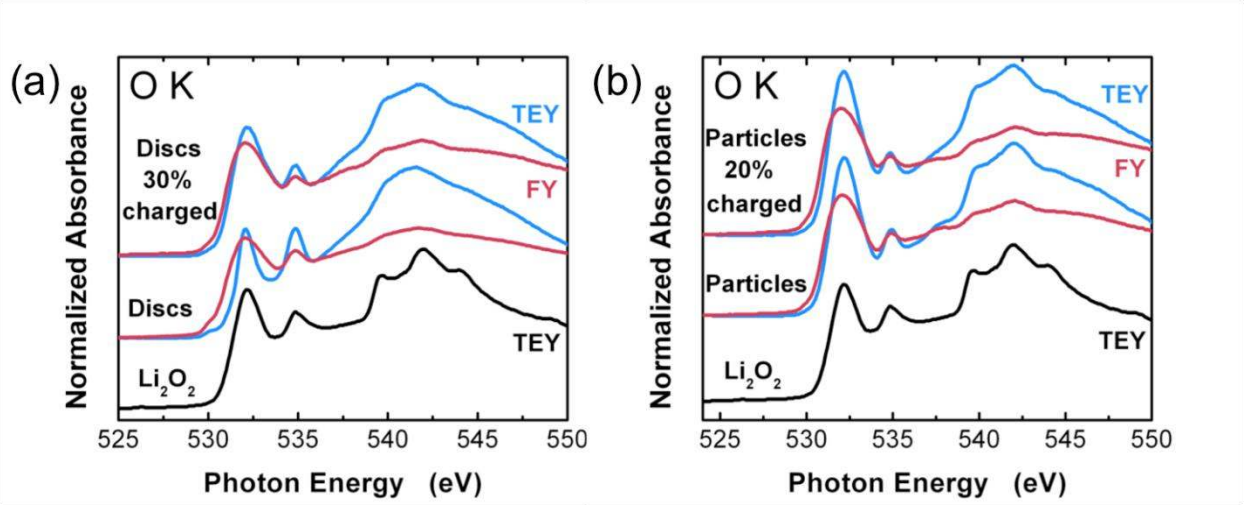

Figure S5. XANES O K-edge data comparing TEY and FY data of discharged and charged Li_2O_2 (a) disc morphologies and (b) particle morphologies with that of reference commercial Li_2O_2. The electrodes are the same as those shown in Fig. 4c, with experimental conditions and electrochemical data given in Fig**.** S7.

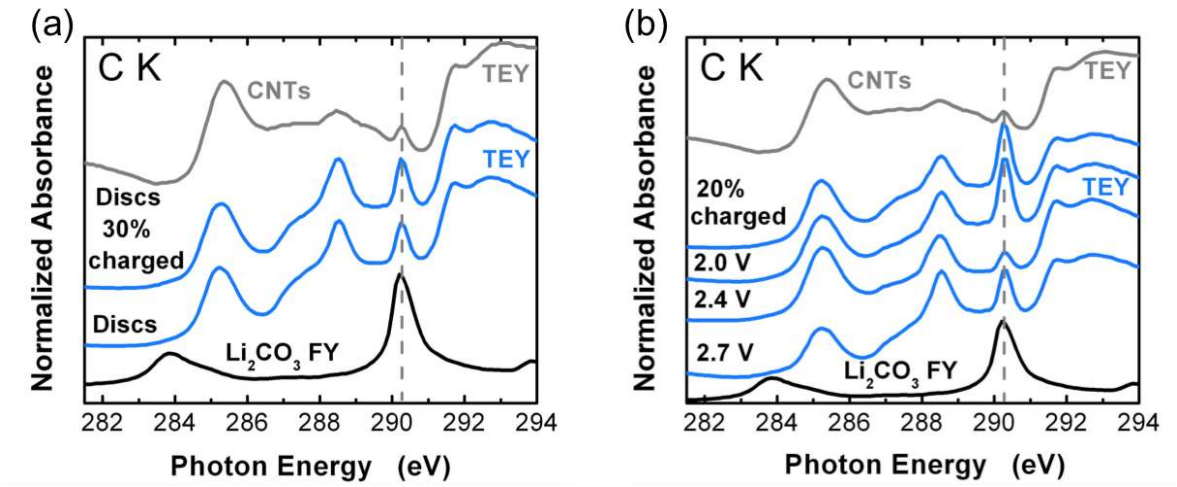

Figure S6. XANES TEY C K-edge spectra of discharged and partially-charged discs (a) and particles (b) and comparison with commercial Li_2CO_3 FY data. Electrochemical details and discharge/charge data from the corresponding electrodes are shown in Fig. S7.

This journal is © The Royal Society of Chemistry 2013

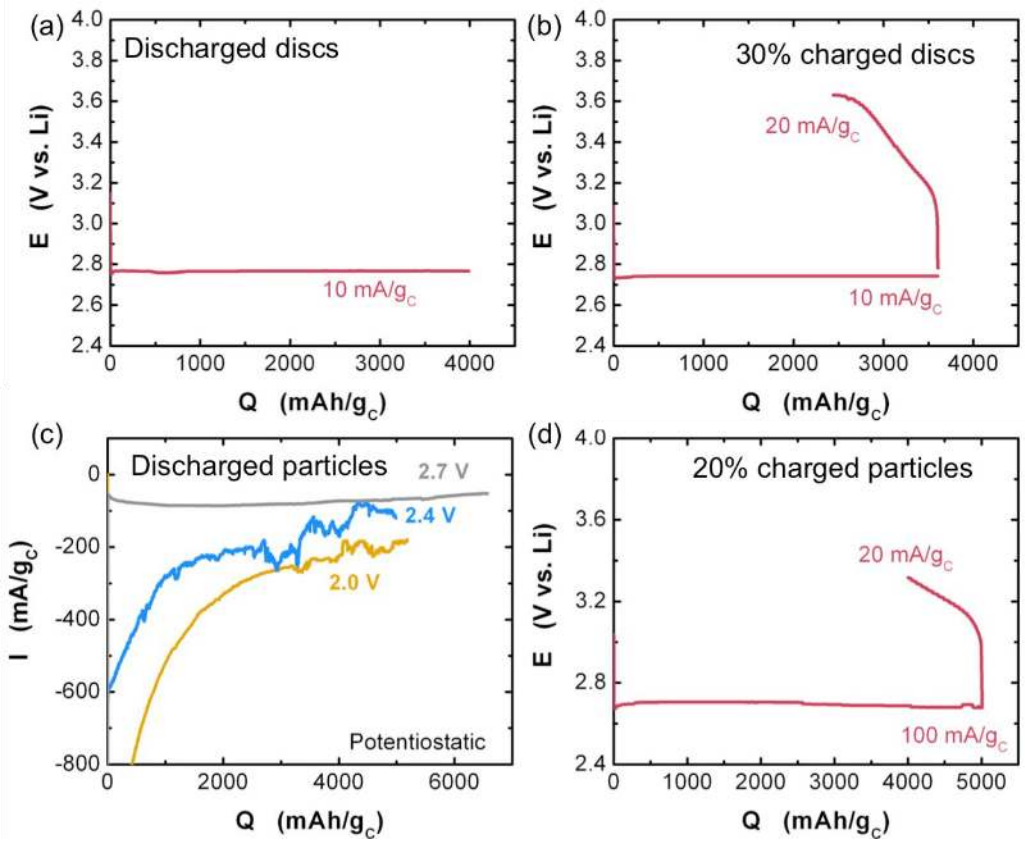

Figure S7. Discharge data of XANES samples used in Fig. 4 and S5-6. (a) Galvanostatic discharge at 10 mA/g_C to 4000 mAh/g_C, forming disc morphologies. (b) Galvanostatic discharge at 10 mA/g_C to 3600 mAh/g_C, forming discs, followed by a ~30% charge at 20 mA/g_C to 2400 mAh/g_C at the onset of the plateau region. (c) Potentiostatic discharge at 2.7, 2.4, and 2.0 V to 6200, 5000, and 5200 mAh/g_C, respectively, forming particle morphologies. (d) Galvanostatic discharge at 100 mA/g_C to 5000 mAh/g_C, forming particles, followed by 20% charging at 20 mA/g_C to 4000 mAh/g_C in the sloping region.

This journal is © The Royal Society of Chemistry 2013

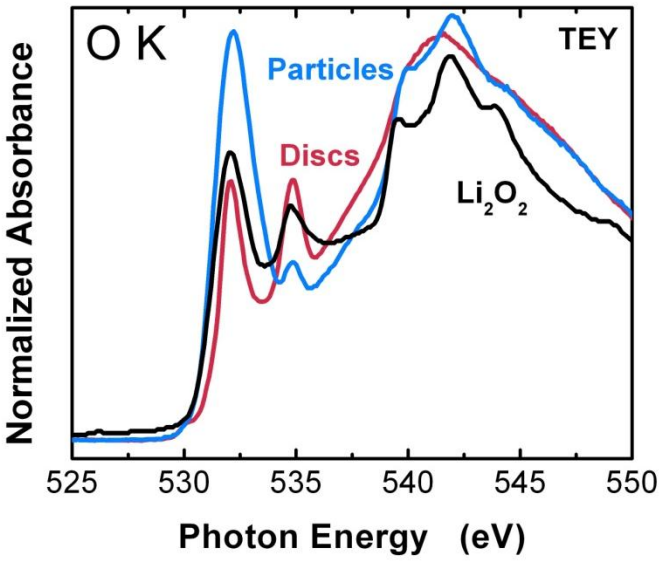

Fig S8. XANES O K-edge TEY spectra overlay of the data in Fig. 4a.

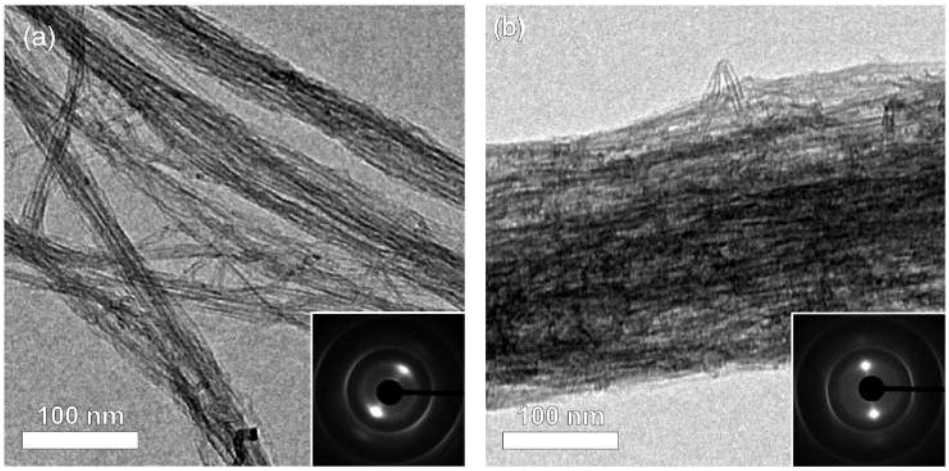

Figure S9. TEM of fully charged electrodes at 20 mA/g_C following (a) discharge at E = 2.0 V vs. Li to 1000 mAh/g_C, forming Li_2O_2 particle morphologies and (b) discharge at E = 2.76 V vs. Li to 1000 mAh/g_C, forming Li_2O_2 disc morphologies. Insets: selected area electron diffraction patterns of the electrode areas shown in (a) and (b) indicating only reflections from CNTs in the charged electrodes. Bundling of the CNTs in the charged samples is due to collapse of the structure from solvent evaporation after removal from the cell. Scale bars: 100 nm.

This journal is © The Royal Society of Chemistry 2013

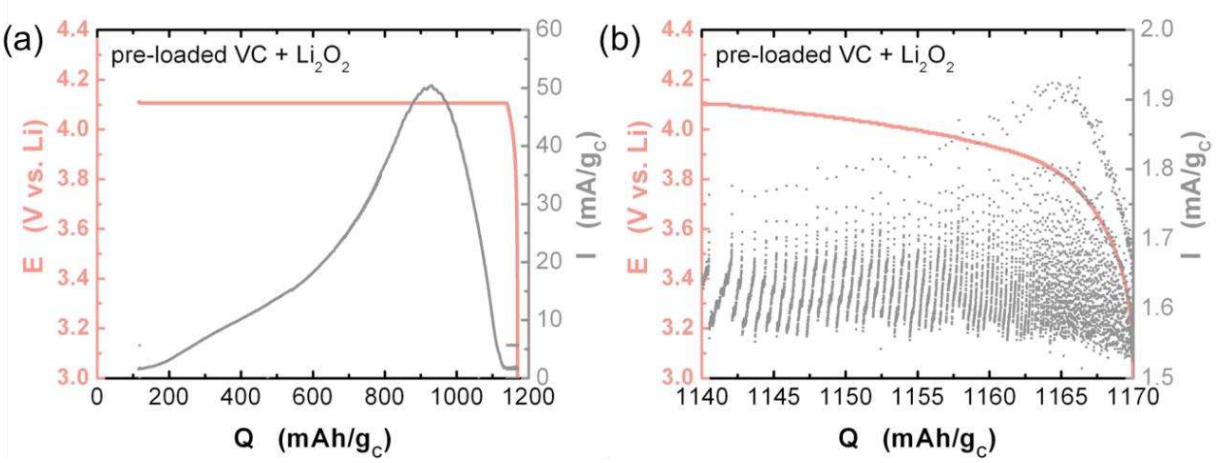

Figure S10. PITT charging of Vulcan carbon electrodes pre-loaded with commercial Li_2O_2. Details regarding electrode fabrication and characterization can be found elsewhere.[2] (a) shows the entire capacity range (normalized to carbon), which is dominated by two-phase oxidation as indicated by the large current rise to ~50 mA/g_C and subsequent decay, and (b) shows the delithiation behavior at the very early stages of charge (for Q > 1140 mAh/g_C; the maximum capacity expected from pre-loaded Li_2O_2 electrodes is 1170 mAh/g_C).

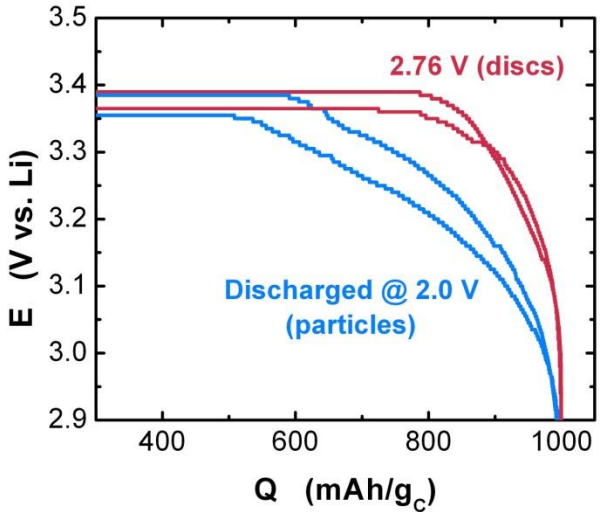

Figure S11. PITT comparison of two different electrodes containing Li_2O_2 particles (discharged potentiostatically at 2.0 V vs. Li to 1000 mAh/g_C) with two electrodes containing Li_2O_2 discs (discharged potentiostatically at 2.76 V vs. Li to 1000 mAh/g_C).

This journal is © The Royal Society of Chemistry 2013

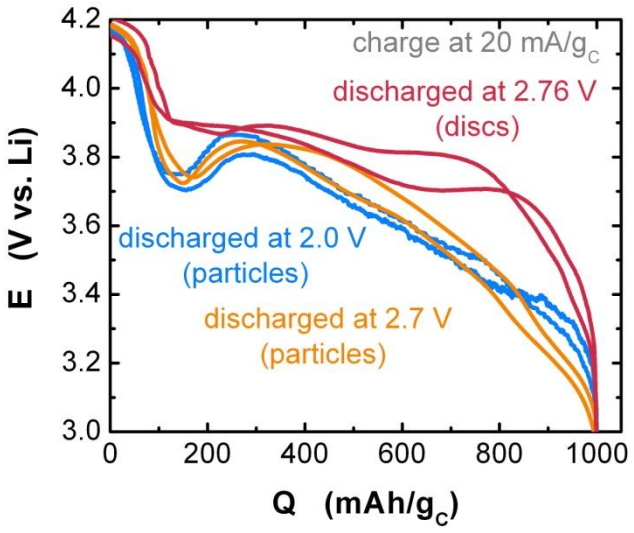

Figure S12. Charging data at 20 mA/g_C for electrodes discharged potentiostatically at 2.0, 2.7 and 2.76 V vs. Li to 1000 mAh/g_C, showing reproducibility of the characteristic charging profiles.

This journal is © The Royal Society of Chemistry 2013

Calculation of the Chemical Diffusion Coefficient, $\tilde{D}$

The chemical diffusion coefficient, $\tilde{D}$, was calculated from PITT charging data (Fig. 7) in the sloping voltage region where the current exhibits a monotonic delithiation-related current decay. Calculations were performed following the process outlined by Wen et al.[3] for delithiation in planar LiAl electrodes (i.e. 1-D diffusion) and were subsequently modified to consider the case of 3D spherical diffusion as outlined by Deiss[4] and by Montella.[5] Although the morphologies of Li_2O_2, particularly the small particles, are clearly three-dimensional, it is possible that one-dimensional diffusion could have relevance for discs given the large anisotropy of Li_2O_2 discs and unknown diffusion mechanisms. Since the mechanistic details of diffusion processes occurring in the discs and particles (e.g., whether isotropic or anisotropic) are not known, we provide both analyses to give reasonable bounds on the diffusion coefficient.

Starting with Fick's first law of diffusion,

$$I(t) = -zFSD\left(\frac{\partial C}{\partial x}\right)_{x=0}$$

where z is the charge transferred per diffusing species, S is the surface area of Li_2O_2, and x = 0 is defined at the Li_2O_2 surface. The solution at short time is given by

$$I(t) = zFS\Delta c\left(\frac{D}{\pi t}\right)^{1/2}$$

where Δc is the change in concentration at the surface of Li_2O_2 following application of the potential step. Assuming negligible ohmic losses, electrolyte mass transport, or kinetic limitations due to small polarizations (ΔE = 5 mV for PITT), Δc is given by:

$$\Delta c = \frac{Q}{zFV}$$

where Q is the total charge transferred per PITT step and V is the volume of the Li_2O_2 particle. Combining terms, the time response is given by

$$I(t) = Q\left(\frac{S}{V}\right)\left(\frac{D}{\pi t}\right)^{1/2}$$

and depends on the ratio of S/V (surface area to volume of Li_2O_2) for the geometry assumed.[4, 5] For a spherical particle, L/V is given by (3/r) where *r* is the particle radius, while for a 1D film, S/V = 1/t where *t* is the film thickness. *r* or *t* can be estimated experimentally using the characteristic diffusion length *L*, which in turn is estimated from knowledge of the crystallite size (in our analysis, L was assumed to be one half the crystallite size measured from XRD in Fig. 3b; errors related to uncertainties in L are shown in Fig. S14). A plot of I(t) vs. $t^{-1/2}$ for a given PITT

This journal is © The Royal Society of Chemistry 2013

current decay response after polarization of ΔE = 5 mV yields a linear region at short times (t << L^2/D, Fig. S13b) from which the value of $\tilde{D}$ can be obtained from the slope, *k*, as

$$\tilde{D}_{planar} = \pi\left(\frac{kL}{Q}\right)^2$$

or

$$\tilde{D}_{spherical} = \frac{\pi}{9}\left(\frac{kL}{Q}\right)^2.$$

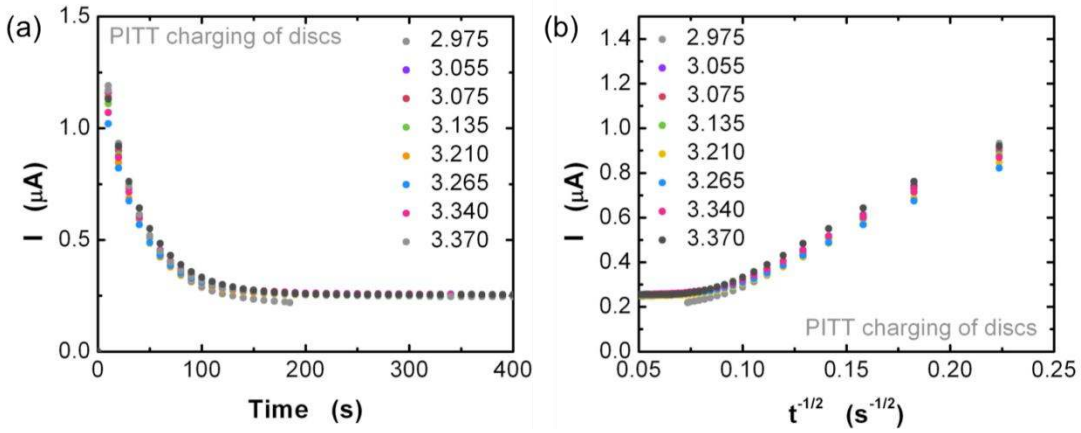

Fig. S13. (a) Raw current vs. time response for a select set of representative PITT steps (ΔE = 5 mV, i_{cutoff} = 0.5 mA/g_C) obtained during charging of Li_2O_2 discs (Fig. 7). The legend indicates the PITT potential applied in V vs. Li. (b) shows the data in (a) plotted as a function of $t^{-1/2}$. The linear region at short times (> 0.1 $s^{-1/2}$) was used to determine the slope from which $\tilde{D}$ was calculated using the process outline above. A diffusion length of 7.5 nm or 12.5 nm was assumed for particles or discs, respectively, which was roughly half the typical crystallite size of each morphology measured from XRD (Fig. 3; ~25 nm crystallite size for discs and ~15 nm crystallite size for particles). The PITT current response of particles was shown to yield similar results as (a) for the discs and is not shown.

This journal is © The Royal Society of Chemistry 2013

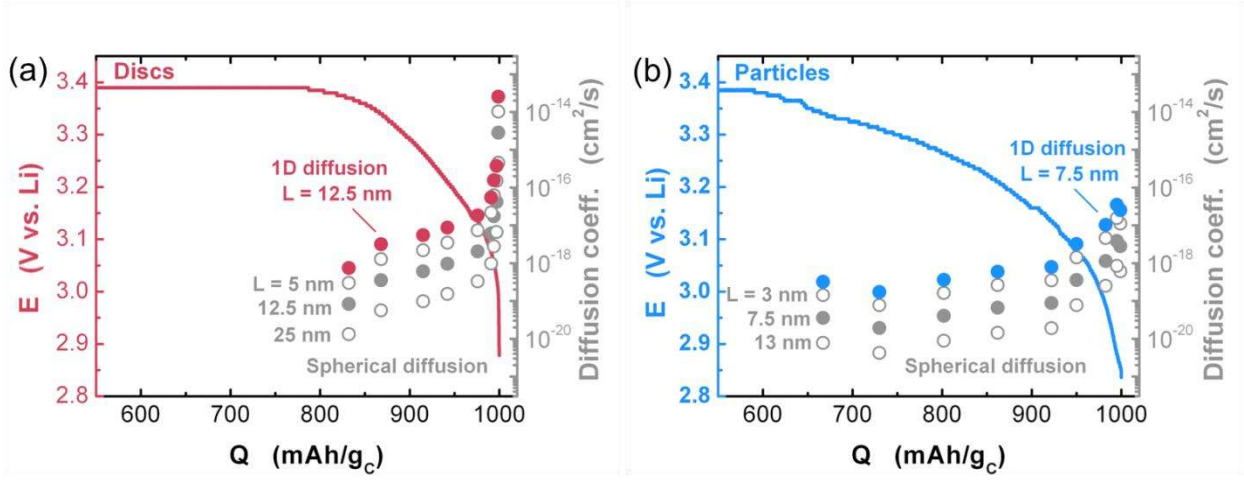

Fig. S14. Chemical diffusion coefficient, $\tilde{D}$, of (a) discs and (b) particles overlaid with the PITT charging profile as a function of capacity. To investigate the error associated with assumption of the characteristic diffusion length L in spherical diffusion, the obtained $\tilde{D}$ for reasonable upper and lower bounds of L for discs and particles are included (gray filled or open symbols). While uncertainty in L may result in slightly shifted (higher or lower) values of $\tilde{D}$ within an order of magnitude, the observed trends (i.e., a decrease in $\tilde{D}$ during delithiation on charge, and a higher maximum $\tilde{D}$ for discs compared to particles) is still observed. The filled colored symbols show $\tilde{D}$ if 1D diffusion is assumed.

References

1. B. D. Cullity and S. R. Stock, *Elements of X-Ray Diffraction*, Prentice Hall, Upper Saddle River, NJ (2001).
2. J. R. Harding, Y.-C. Lu, Y. Tsukada and Y. Shao-Horn, *Physical Chemistry Chemical Physics*, **14**, 10540 (2012).
3. C. J. Wen, C. Ho, B. A. Boukamp, I. D. Raistrick, W. Weppner and R. A. Huggins, *International Metals Reviews*, **5**, 253 (1981).
4. E. Deiss, *Electrochim Acta*, **47**, 4027 (2002).
5. C. Montella, *Electrochim Acta*, **51**, 3102 (2006).